



Treatment of Hexavalent Chromium Contaminated Wastewater Using Activated Carbon Derived from Coconut Shell Loaded by Silver Nanoparticles: Batch Experiment

Lan Huong Nguyen · Thi Minh Phuong Nguyen · Huu Tap Van · Xuan Hoa Vu · Thi Lan Anh Ha · Thi Hong Vien Nguyen · Xuan Hoan Nguyen · X.C. Nguyen

Received: 21 November 2018 / Accepted: 11 February 2019 / Published online: 22 February 2019
© Springer Nature Switzerland AG 2019

Abstract Chromium (Cr(VI)) causes serious impacts on the environment and human. In this study, the commercial activated carbon-loaded silver nanoparticle (AgNPs-AC) was used as a new adsorbent to remove Cr(VI) from the aqueous solution. Batch adsorption experiments were conducted to evaluate the effects of pH, the initial concentration of Cr(VI), contact time, and dose of AgNPs-AC upon removal of Cr(VI) from the aqueous solution. The results showed that at pH of 4, the contact time of 150 min, 40 mg/L of initial Cr(VI), and dosage of 20 mg AgNPs-AC/25 mL were the most suitable condition for adsorption of Cr(VI) onto AgNPs-AC from the

aqueous solution. The maximum adsorption capacity achieved at abovementioned conditions was 27.70 mg/g. Meanwhile, the adsorption capacity of commercial activated carbon from a coconut shell obtained only 7.61 mg/g in the case where the initial Cr(VI) concentration is 10 mg/L and the contact time is 60 min. The adsorption kinetic data were found to fit best to the pseudo-second-order model with a high correlation coefficient ($R^2 = 0.9597$). The adsorption process was controlled by chemisorption due to the appearance of new chemical species on the adsorbent surface. The positively charged functional groups rapidly reduced Cr(VI) to Cr(III), and Cr(III) was

L. H. Nguyen · X. H. Nguyen
Faculty of Environment – Natural Resources and Climate Change,
Ho Chi Minh City University of Food Industry (HUFI), 140 Le
Trong Tan Street, Tay Thanh Ward, Tan Phu District, Ho Chi Minh
City, Vietnam

T. M. P. Nguyen
Faculty of Environment and Chemical Engineering, Duy Tan
University (DTU), 254 Nguyen Van Linh Road, Da Nang,
Vietnam

H. T. Van · T. H. V. Nguyen
Faculty of Natural Resources and Environment, Thai Nguyen
University of Sciences (TNUS), Tan Thinh Ward, Thai Nguyen,
Vietnam

X. H. Vu
Faculty of Physic and Technology, Thai Nguyen University of
Sciences (TNUS), Tan Thinh ward, Thai Nguyen City, Vietnam

T. L. A. Ha
Advanced Education Program Office, Thai Nguyen University of
Agriculture and Forestry (TUA), Quyet 17 Thang Ward, Thai
Nguyen City, Vietnam

X. Nguyen
Laboratory of Advanced Materials Chemistry, Advanced Institute
of Materials Science, Ton Duc Thang University, Ho Chi Minh
City, Vietnam

X. Nguyen (✉)
Faculty of Applied Sciences, Ton Duc Thang University, Ho Chi
Minh City, Vietnam
e-mail: nguyensexuanca@tdtu.edu.vn

subsequently adsorbed by the carboxyl group on the adsorbent's surface. From this study, it can be concluded that AgNPs-AC is a fully promising, low-cost adsorbent in the removal of Cr(VI) from the aqueous solution.

Keywords AgNPs-AC · Adsorption · Activated carbon · Hexavalent chromium · Silver nanoparticles

1 Introduction

Trace metals are major pollutants found in marine, groundwater, industrial wastewater, and even in treated wastewaters (Demir and Arisoy 2007). In water and wastewater, Cr(VI) can exist in the forms of chromate (CrO_4^{2-}), hydrogen chromate (HCrO_4^-), dichromate ($\text{Cr}_2\text{O}_7^{2-}$), and hydrogen dichromate (HCr_2O_7^-) (Elfeky et al. 2017; Huang et al. 2015). The highest exposure to hexavalent chromium is caused by electronic components manufacturing, paint manufacturing, mechanical alloying, tanning of animal hides, and metallurgical (Álvarez-Ayuso et al. 2007; Lu et al. 2017; Sheth and M Soni 2005). Cr(VI) is extremely harmful to human health and ecosystems because of its high mobility in soil and water, and its propensity to accumulate in plants and animals through food chains (Kera et al. 2017; Saha et al. 2011). Cr(VI) results in skin irritation, epigastric pain, severe diarrhea, and lung cancer (Kumar and Meikap 2014; Sheth and M Soni 2005; Singh 2017). United States Environmental Protection Agency (EPA) established the allowed maximum contaminated level of Cr^{6+} in a drinking and potable water to be 0.1 mg/L and 0.5 mg/L, respectively (EPA 1983). Thus, Cr(VI) needs removing before being discharged in receiving sources.

Popular technologies have been applied to remove Cr(VI) from the aqueous solutions including chemical reduction, chemical precipitation, ion exchange, membrane separation, and adsorption (Álvarez-Ayuso et al. 2007; Kumar and Meikap 2014; Li et al. 2017; Owalude and Tella 2016). Among such existing methods, adsorption is an effective and low-cost method for removing Cr(VI) from water and wastewater. Recently, nanotechnology is a rapidly growing scientific field in producing and constructing devices. Besides,

nanomaterials were also used as an efficient adsorbent to remove pollutants from water and wastewater due to an extremely high surface area. The studies about using nanomaterials in the removal of pollutants were performed such as the removal of Cr(VI) by $\text{MoS}_2/\text{Fe}_3\text{O}_4/\text{nZVI}$ nanocomposites (Lu et al. 2017), magnetic multi-wall carbon nanotubes (Huang et al. 2015), and magnetic nanocomposite (Elfeky et al. 2017; Kera et al. 2017). However, nanomaterials are still high cost, and the application of nanomaterials in wastewater treatment is quite limited. Thus, the studies should focus on a combination of the nanomaterials with low-cost adsorbents to reduce treatment cost and enhance widely application of nanomaterials the in removal of pollutants. Recently, the studies in the modification of commercial activated carbon by loading various nanomaterials to improve surface area of adsorbents in the removal of heavy metals from the aqueous solution were investigated by some scholars, including activated carbon-loaded zero valent metals to adsorb chromium ion (Kakavandi et al. 2014), Cr(VI), Cu, and Cd (Jain et al. 2018) from the aqueous solution; the gold nanoparticle-loaded activated carbon was used to remove Congo red (Ghaedi et al. 2011); the zinc oxide nanoparticle was loaded on the activated carbon for the removal of uric acid (Marahel et al. 2015). Silver nanoparticle was also loaded on the activated carbon for the removal of methyl orange (Karimi 2012), methylene blue (Ghaedi et al. 2018, Van et al. 2018a, b), and *Staphylococcus aureus* and *Escherichia coli* (Tang et al. 2017). However, the studies about the modification of commercial activated carbon by loading silver nanoparticles to make a newly modified adsorbent in removing Cr(VI) from the aqueous solution are quite scarce. This study, thereby, was to develop a new adsorbent (AgNPs-AC) from a coconut shell activated carbon fully loaded AgNPs to remove Cr(VI) from the aqueous solution. The physicochemical properties of the new adsorbent (AgNPs-AC) were characterized by SEM, XRD, and FTIR. The effects of impregnation ratio (w/w) of activated carbon and AgNPs, pH solution, adsorption time, adsorbent dosage, and initial concentrations of hexavalent chromium on the adsorption capacity of Cr(VI) by AgNPs-AC were investigated in batch experiments. The adsorption isotherm, adsorption kinetics, and

adsorption mechanisms of Cr(VI) on AgNPs-AC were studied under found optimal conditions.

2 Materials and Methods

2.1 Chemical

All chemicals, including potassium dichromate ($K_2Cr_2O_7$), $AgNO_3$, NaOH, and H_2SO_4 were purchased from Merck (Darmstadt, Germany). Commercial granular activated carbon (AC) with a particle size of 1 to 2 cm was purchased from Tra Bac Company, Vietnam. A stock solution of chromium (Cr(VI)) with a concentration of 1000 mg/L was prepared by dissolving 0.7024 g of potassium dichromate ($K_2Cr_2O_7$) in 250 mL of double distilled water. The working solutions were prepared by diluting the stock solution with a double distilled water to the desired concentrations.

2.2 Synthesis of Silver Nanoparticles

Silver nanoparticles were made from silver nitrate ($AgNO_3$) by the hydrothermal method (Tang et al. 2017). Firstly, 100 mL of $AgNO_3$ solution (0.001 M) was mixed with 0.2 g of starch to generate starch solutions containing Ag^+ ions. The solution was continuously stirred vigorously on a magnetic stirrer at 70 °C to ensure the complete homogeneousness of the mixture. The temperature of the solution was maintained at 70 °C, and 25 ml of sodium borohydrides (0.001 M) was gradually added (drop by drop) into the mixture. Finally, the obtained solution was cooled to room temperature for further use.

2.3 Preparation of the AgNPs-Loaded Activated Carbon (AgNPs-AC)

Commercial activated carbon (AC) with a particle size less than 0.5 mm was prepared by washing and drying at 105 °C for 2 h in an oven. The impregnation method was used to load AgNPs on AC by mixing AC with AgNPs at a various mass ratio (0.5–3% w/w of AC and AgNPs) in flasks (Salem et al. 2018). The flasks were then shaken at 120 rpm orbital for 24 h in the dark. After impregnation, the wet samples were filtered and dried for 2 h at 105 °C in an oven to obtain activated carbon modified by silver nanoparticles (AgNPs-AC). The AgNPs-AC with an average particle size less than

0.5 mm was used in the batch-mode adsorption experiments to remove Cr(VI) from the aqueous solution.

2.4 Characterization of AgNPs-AC

Physicochemical properties of adsorbents (AC and AgNPs-AC) were determined by an energy dispersive X-ray spectroscopy (Hitachi S-4800) with EDS and SEM systems and X-ray diffraction pattern (XRD-D8 ADVANCE). The surface functional groups of AC and AgNPs-AC were detected using a Fourier transform IR-6300 in a/IR-6300) in a 500–4000 cm^{-1} range. The pH at the point of zero charge (pH_{PZC}) was determined by the drift method (Tran et al. 2016), the BET surface area of AC and AgNPs-AC was measured by a pore size and specific surface area analyzer (BET, Builder, SSA-4300).

2.5 Batch Adsorption Experiments

Batch experiments were conducted to evaluate the effects of various parameters on the adsorption capacity of AgNPs-AC for Cr(VI). In these experiments, the activated carbon-loaded by silver nanoparticles (AgNPs-AC) at an obtained optimal impregnation ratio from the above experiment was placed into a 50-mL conical flasks containing 25 mL of $K_2Cr_2O_7$ solution with initial concentrations of Cr(VI) in a range from 5 to 80 mg/L with varying experimental parameters, including pH (3–10), contact time (5–210 min), and adsorbent dose (10–100 mg AgNPs-AC/25 mL Cr(VI)) on adsorption of Cr(VI) on AgNPs-AC. The flasks, then, were shaken at 120 rpm orbital for 60 min by a shaker machine (PH-2A, China) at room temperature (25 ± 2 °C) in the laboratory. All experiments were parallely performed.

2.6 Measurements

The Cr(VI) concentrations in the bulk reactor suspensions of all samples in the above experiments were measured. Chromium was measured by the colorimetric method on Atomic Absorption Spectrometry (AAS) (Hitachi Z 2000, Japan). The pH was measured by a pH meter (Hanna HI 9025 Romania). The amounts of chromium adsorbed onto AgNPs-AC at equilibrium (q_e ; mg/g) and any time t (q_t ; mg/g) were calculated according

to a mass balance equation as shown below:

$$q_e = \frac{(C_o - C_e)V}{W} \quad (1)$$

$$q_t = \frac{(C_o - C_t)V}{W} \quad (2)$$

where C_o (mg/L), C_t (mg/L), and C_e (mg/L) are the hexavalent chromium concentrations in the solution at beginning time, any time t , and equilibrium, respectively; V (L) is the working volume of hexavalent chromium solution; and W (g) is the dry weight of used AgNPs-AC.

2.7 Data Analysis

All experiments were done in triplicate. All data statistics, comprising means, standard deviations, relative standard deviations, and regressions (linear), were computed on SPSS software version 19.0. Wherever possible, the error bars indicating the standard deviation are illustrated in all figures.

3 Results and Discussion

3.1 Characterization of Activated Carbon-Loaded Silver Nanoparticles (AgNPs-AC)

The SEM from Fig. 1 shows that stable and porous surface structures are one of the characteristics that affected the adsorption capacity of AC. Figure 1a shows the porous AC surface structure with a high Brunauer–Emmett–Teller (BET) specific surface area of 691.64 m²/g and a total pore volume of 0.062 cm³/g. Figure 1b indicates the structure of activated carbon-loaded silver nanoparticles (AgNPs-AC 2% w/w) with a negligible increase in surface area of 701.65 m²/g and a pore volume of, almost equal, about 0.061 cm³/g. The results suggested that AgNPs-loaded play a more important role in Cr(VI) adsorption than the specific surface area of AC.

The presence of silver nanoparticles was observed with white circle shapes in Fig. 1b which did not occur in Fig. 1a. This indicates that silver nanoparticles were successfully loaded onto the activated carbon's surface and the sponginess increased significantly.

The surface characteristics prove high adsorption capacity of AgNPs-AC through mass transport inside the adsorbent. Figure 1c presents EDS analysis, and it shows the presence of C (91.87%) and O (8.13%) elements while Fig. 1d shows that the proportions of elements for C, O, and Ag were 99.14%, 0.76%, and 0.1%, respectively. And the presence of these elements could have an effect on the adsorption mechanism. Figure 1a, b shows a significant difference between the surface before and after activation of AC with silver nanoparticles. And the attributed reasons were that a high percent of voids are being occupied by the volatile matters. In this case, the silver nanoparticles were successfully attached to the AC's surface.

The crystal structure and phase purity of the prepared silver nanoparticles were identified by measuring the XRD pattern as shown in Fig. 2. Most characteristic peaks were well indexed to amorphous with a high graphite crystal structure in the XRD spectra of AC (Fig. 2a) and AgNPs-AC (Fig. 2b). XRD results of AC from Fig. 2a indicate that the broad peak occurred at 30.09° and 61.93°, and at 22.63° in the case of AgNPs-AC (Fig. 4). It proved that carbon graphite was present in both AC and AgNPs-AC. In the XRD spectra of AgNPs-AC (Fig. 2b), the silver nanoparticles appeared on the AC's surface at the peak of 38.19° and 44.33°. This result agreed with the previous reports when the silver nanoparticles were loaded on activated carbon and they occurred at the peaks of 38.17° and 44.21° (Karimi 2012), 44° (Altintig et al. 2016).

Figure 3 presents FTIR spectrum of AC and AgNPs-AC. From Fig. 3, it can be seen that the presence of O–H stretch bonded group appeared at peaks of 3822, 3720, and 3406 cm⁻¹. The reports of De Castro et al. (2018) and Anisuzzaman et al. (2015) also indicated similar results that the O–H group appeared at peaks around 3200–3800 cm⁻¹. A peak of 1669 cm⁻¹ shows C=O stretching vibration in carbonyls, including ketones, aldehydes, lactones, and carboxylic groups (Altintig et al. 2016; Anisuzzaman et al. 2015). The C=C stretching vibration in aromatic rings appeared at the peak of 1514 cm⁻¹ (Foo and Hameed. 2009). At the strong peak of 1050 cm⁻¹, the frequency shows the C–O stretching of carboxylic acids or lactone groups (Altintig et al. 2016; Lazim et al.

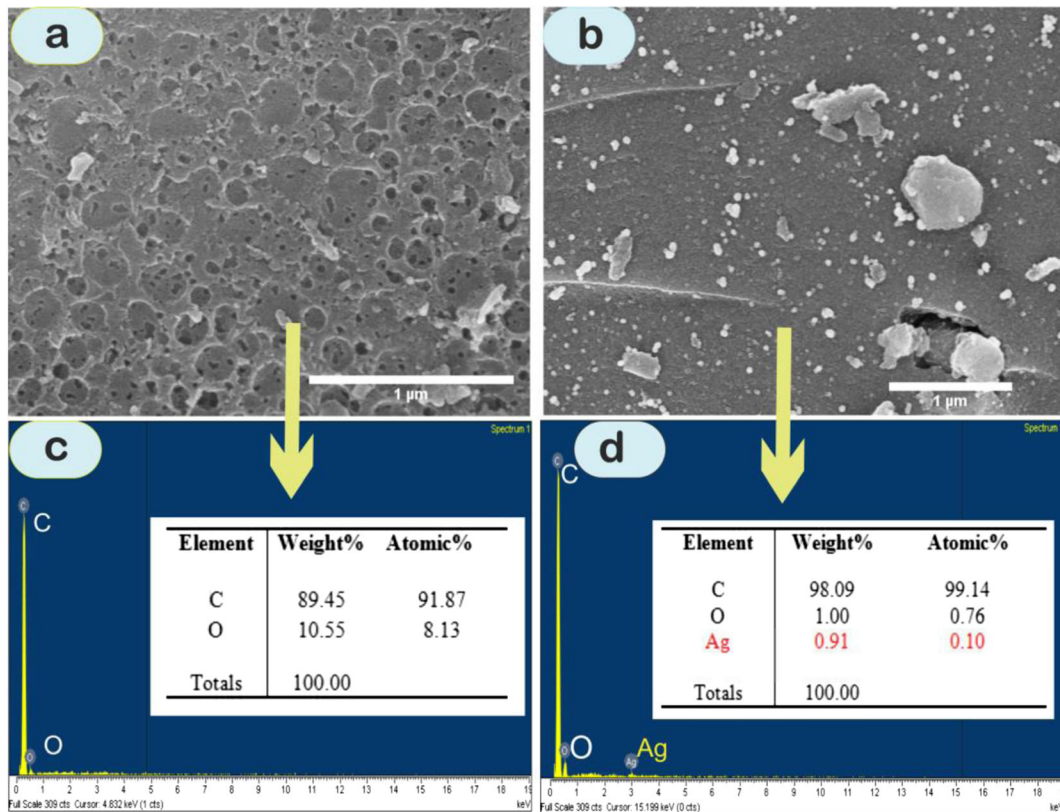


Fig. 1 SEM image of (a) AC and (b) AgNPs-loaded activated carbon (AgNPs-AC), EDS spectra of (c) AC and (d) AgNPs-loaded activated carbon (AgNPs-AC)

2015) and the presence of aromatic C–H at the peaks of 581–841 cm^{-1} (Anisuzzaman et al. 2015). The pH_{PZC} of AC was 4.13 and pH_{PZC} of AgNPs-AC before and after the adsorption process were

found to be 5.09 and 4.80, respectively (Fig. 4). The analysis results show that the pH_{PZC} of AgNPs-AC did not significantly change before and after the adsorption process.

Fig. 2 XRD graph of (a) activated carbon from coconut shells (AC) and (b) AgNPs (2%)-loaded activated carbon (AgNPs-AC)

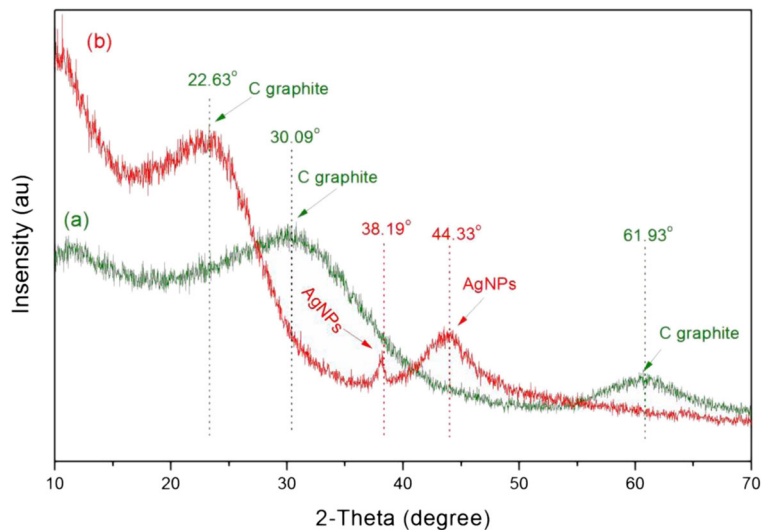
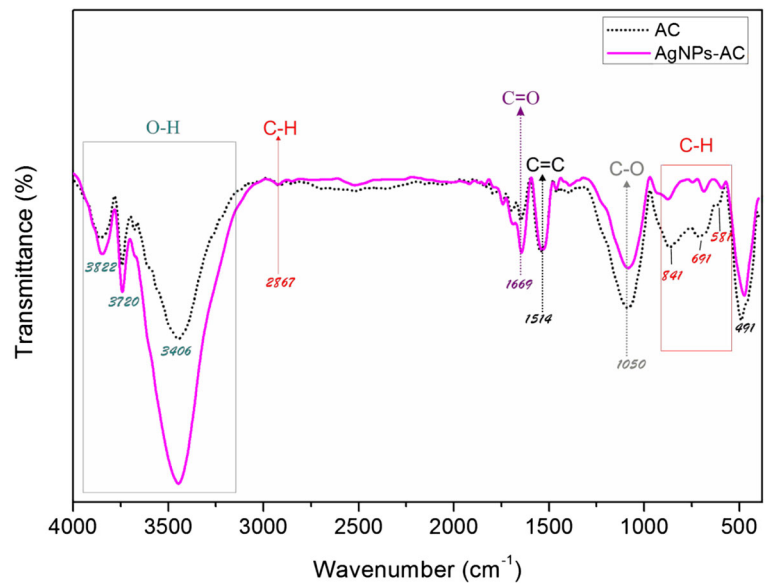


Fig. 3 FTIR graph of AC and AgNPs-AC



3.2 Effect of Impregnation Ratio (AgNPs/AC) on Cr(VI) Adsorption Capacity

The initial experiments were conducted to compare the adsorption capacity of AC with AC-loaded by AgNPs at a varying mass ratios between AgNPs and AC (0.5%, 1.0%, 1.5%, 2.0%, 2.5%, 3.0%) with the initial Cr(VI) concentration of 10 mg/L at room temperature ($25 \pm 2^\circ\text{C}$). The results were presented in Fig. 5.

From Fig. 5, it was clear that Cr(VI) adsorption capacity increased with an increase in the impregnation ratio of AgNPs/AC from 0.5 to 2.0%. And the removal efficiency of Cr(VI) was correspondingly obtained from 30.77 to 40.00%. The Cr(VI)

adsorption capacity reached a maximum value of 10.33 mg/g with a maximum removal efficiency of Cr(VI) of 40% at the impregnation ratio of AgNPs-AC of 2% that was much higher than that of AC only. This can be explained due to the effect of the silver nanoparticles loaded on AC (Figs. 1 and 2) leading to an increase in adsorption capacity. However, the adsorption capacity did not continuously increase when increasing the impregnation ratio. Based on the above results, the optimum impregnation ratio to load AgNPs onto AC was 2% (w/w). In conclusion, AgNPs-AC at the impregnation ratio of 2% (w/w) is most suitable and is used for subsequent experiments.

Fig. 4 pH_{PZC} of AC and AgNPs-AC before and after adsorption process of Cr(VI)

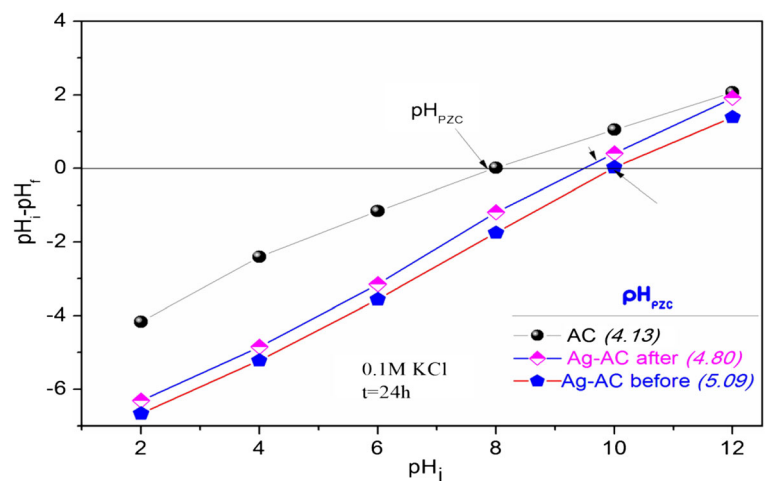
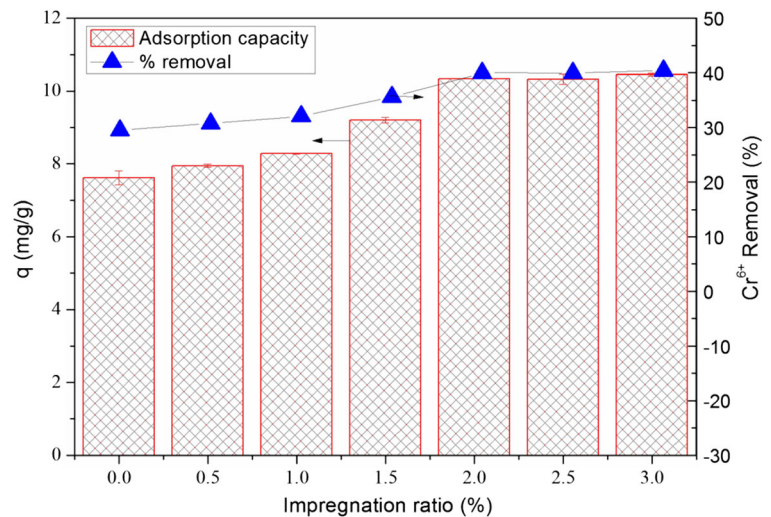


Fig. 5 The effect of the various impregnation ratios between AgNPs and AC on the adsorption capacity of Cr(VI) at an initial Cr(VI) concentration of 10 mg/L, an adsorbent dose of 10 mg AgNPs-AC/25 mL Cr(VI) solution, and contact time of 60 min



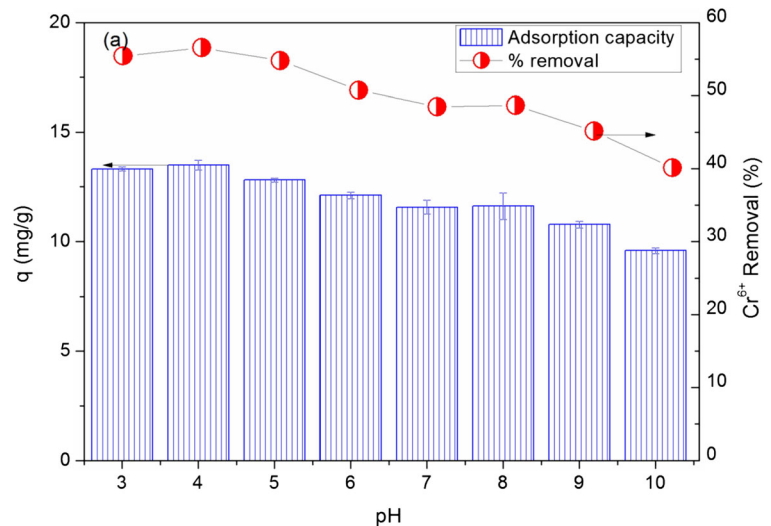
3.3 Effect of pH

Experiments were carried out at various pH solutions (3, 4, 5, 6, 7, 8, 9, and 10) with an initial Cr(VI) concentration of 10 mg/L at room temperature (25 ± 2 °C). The results of the effect of pH solution on the adsorption capacity of Cr(VI) by AgNPs-AC are presented in Fig. 6. Figure 6 indicated that the adsorption capacity of Cr(VI) on AgNPs-AC strongly depends on the pH solution. At low pH, the Cr(VI) removal efficiency is higher than that of at high pH (Singh 2017). The highest removal efficiency of Cr(VI) reached a pH solution from 3 to 4. The adsorption capacity decreased when increasing the pH from 5 to 10. The Cr(VI) adsorption capacity reached a maximum value of 13.50 mg/g at pH 4 with a

maximum removal efficiency of Cr(VI) at 56.57%. The results show that Cr(VI) was easily reduced to Cr(III) in an acidic pH. Similar results were found in other scholars' studies (Mitra et al. 2017; Kumar and Jena 2017; Rai et al. 2016), and a similar result was also reported by Kera et al. (2017) that the optimum pH of 4 for the adsorption of Cr(VI) onto magnetic nanoparticles (Fe_3O_4) capped with cetyltrimethylammonium bromide. Additionally, the above FTIR data indicated that the carboxyl groups appeared on the AgNPs-AC surface, thus Cr(III) was subsequently adsorbed by these carboxyl groups (Tran et al. 2016).

The results can be further explained as follows: under oxidizing conditions, the principal Cr(VI) species are HCrO_4^- , CrO_4^{2-} , and $\text{Cr}_2\text{O}_7^{2-}$. Overall, $\text{Cr}_2\text{O}_7^{2-}$ and

Fig. 6 Effect of pH on the adsorption capacity and removal efficiency of Cr(VI) by AgNPs-AC at an initial Cr(VI) concentration of 10 mg/L, contact time of 60 min, and an adsorbent dose of 10 mg AgNPs-AC/25 mL Cr(VI) solution



HCrO_4^- dominate at $\text{pH} < 6.0$ while CrO_4^{2-} dominates at $\text{pH} > 6.0$ (Li et al. 2017). At $\text{pH}_{\text{solution}} < \text{pH}_{\text{PZC}}$ (5.09), the surface of AgNPs-AC becomes positively charged and favors the uptake due to the enhancement of the electrostatic interaction between $\text{Cr}_2\text{O}_7^{2-}$, HCrO_4^- , and the adsorbent. At low pH, the number of protons available on the surface of the adsorbate increased resulting in an attraction between $\text{Cr}_2\text{O}_7^{2-}$, HCrO_4^- , and the adsorbent occurred; thus, water molecules are easier to displace from metal binding sites than hydroxyl groups (Akram et al. 2017; Alvarez et al. 2007). Therefore, at low pH value, electrostatic attraction, and/or by the binding of $\text{Cr}_2\text{O}_7^{2-}$ and HCrO_4^- to acidic functional groups, dominated leading to the higher chromium adsorption onto AgNPs-AC. Meanwhile, when $\text{pH}_{\text{solution}} > \text{pH}_{\text{PZC}}$ (5.09), charges on the surface of adsorbent became negative and the adsorption capacity was inhibited due to the repulsive forces generated between the Cr(VI) ions, and adsorbent resulting in adsorption capacity of Cr(VI) onto AgNPs-AC decreased. The same results have been reported in other recent studies (Kumar and Meikap 2014). From this result, it can be seen that pH is an important parameter that controlled the adsorption capacity of heavy metals from wastewater. In this study, the maximum adsorption capacity of Cr(VI) onto AgNPs-AC took place at pH 4.

3.4 Effect of Contact Time

The effect of contact time on the adsorption capacity and removal efficiency of Cr(VI) by AgNPs-AC was studied at pH 4, 10 mg/L of initial Cr(VI) concentration, and a contact time from 5 to 210 min. The results are presented in Fig. 7. Figure 7 shows that the Cr(VI) adsorption capacity increased with an increase in contact time from 5 to 150 min corresponding with a removal efficiency of Cr(VI) from 21.42 to 62.07%. The Cr(VI) adsorption capacity reached a maximum value of 15.67 mg/g at 150 min with a maximum removal efficiency of Cr(VI) at 62.07%. From 180 to 210 min, the adsorption process remained constant. It can be explained that the active sites on the adsorbent (AgNPs-AC) surface are vacant in the beginning stage, thus adsorption process occurred faster leading to a faster increase in the extent of adsorption. However, the active sites were almost fully occupied with longer residence time and the adsorption and desorption process tend to be equal. And the extent of adsorption slightly decreased and reached nearly constant at equilibrium (Rai et al. 2016). In this study, an

adsorption equilibrium time of 150 min would be used for further experiments. This trend was similar to those reported results by other researchers when investigating the adsorption of Cr(VI) from industrial wastewater by a coffee husk (Berihun 2017) and activated carbon prepared from mango kernel activated with H_3PO_4 (Rai et al. 2016) with an equilibrium time of 150 min.

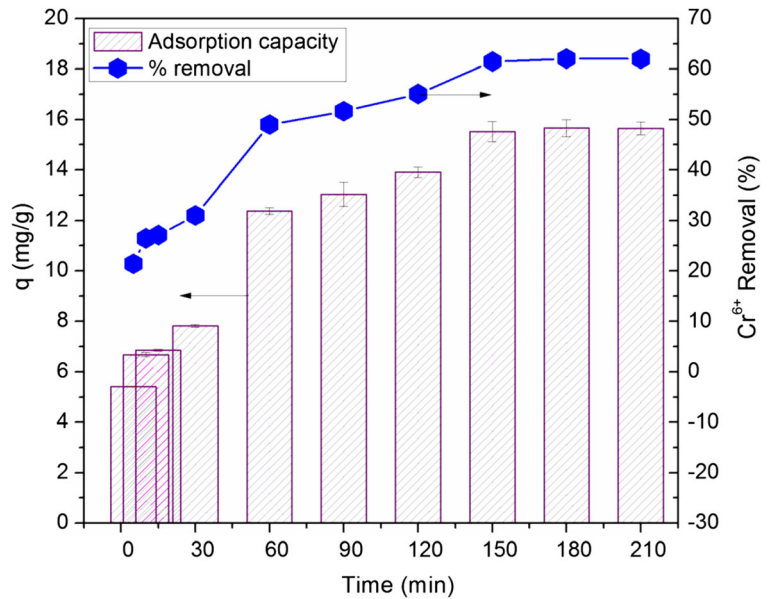
3.5 Effect of Adsorbent Dose

In this study, seven different adsorbent dosages (AgNPs-AC) were selected ranging from 10 to 100 mg while the initial Cr(VI) concentration was fixed at 10 mg/L. The experiments of Cr(VI) adsorption were conducted at an optimum pH of 4 and contact time of 150 min. The results are presented in Fig. 8. From Fig. 8, it can be seen that the adsorption percentage of Cr(VI) onto AgNPs-AC increased significantly from 62.73 to 75.97% and the adsorption capacity increased, respectively, from 31.58 to 38.25 mg/g corresponding with an increase in dosages of AgNPs-AC from 5 to 20 mg/25 mL Cr(VI). These results can be explained that when the adsorbent dose increased, the active sites on AgNPs-AC's surface and the number of adsorbent particles increased and thus more Cr(VI) were attached on the AgNPs-AC surface. Additionally, it can be seen that the adsorption percentage of Cr(VI) decreased very slightly from 75.97 to 70.84% corresponding with an increase in doses of AgNPs-AC from 20 to 60 mg/25 mL. However, the adsorption percentage of Cr(VI) slightly decreased when the amount of AgNPs-AC continued to increase to more than 20 mg/25 mL of solution. This can be explained due to a low surface area of AgNPs-AC leading to a decrease in the adsorption of Cr(VI) onto AgNPs-AC. Thus, the maximum adsorption capacity achieved was 38.25 mg/g with a AgNPs-AC dose of 20 mg/25 mL at 10 mg/L of initial Cr(VI). Similar results have also been reported in other recent studies (Akram et al. 2017; Ali et al. 2016; Huang et al. 2015).

3.6 Effect of Initial Cr(VI) Concentration

The effects of initial Cr(VI) concentration on the adsorption capacity and removal efficiency of Cr(VI) by AgNPs-AC were performed by batch experiments in shaker flasks. The initial Cr(VI) concentrations were changed in range of 5, 10, 20, 30, 40, 50, 60, 70, and 80 mg/L. All experiments were conducted at an optimum pH of 4, contact time 150 min, and a dose of

Fig. 7 Effect of contact time on Cr(VI) adsorption by AgNPs-AC with initial Cr(VI) concentration of 10 mg/L, an adsorbent dose of 10 mg AgNPs-AC/25 mL Cr(VI), and pH solution of 4



AgNPs-AC of 20 mg/25 mL that were determined in the above-described experiments. The flasks were shaken at 120 rpm orbital at room temperature (25 ± 2 °C). The results are illustrated in Fig. 9. It can be seen from Fig. 9 that the adsorption capacity of Cr(VI) by AgNPs-AC increased from 5.13 to 27.70 mg/g with an increase in initial Cr(VI) concentrations from 5 to 40 mg/L and the adsorption capacity remained constant when initial Cr(VI) concentration was continuously increased. However, adsorption efficiency decreased from 82 to 28% when increasing the initial Cr(VI) concentration from 5

to 80 mg/L. Chromium ions in solution act as an important driving force to overcome mass transfer resistance of ions between the aqueous solution and the adsorbent (Akram et al. 2017; Manzoor et al. 2013). At a low initial Cr(VI) concentration, almost Cr(VI) ions interacted with active binding sites. However, with a higher initial Cr(VI) concentration, the number of active adsorption sites is not enough to accommodate the chromium ions leading to the adsorption capacity not increasing. In Manfe’s study, he also reported that the adsorption capacity of Cr(VI) by *Prunus amygdalus*

Fig. 8 Effect of adsorbent dosage on adsorption capacity and removal efficiency of Cr(VI) by AgNPs-AC with an initial Cr(VI) concentration of 10 mg/L, contact time of 150 min, and pH solution of 4

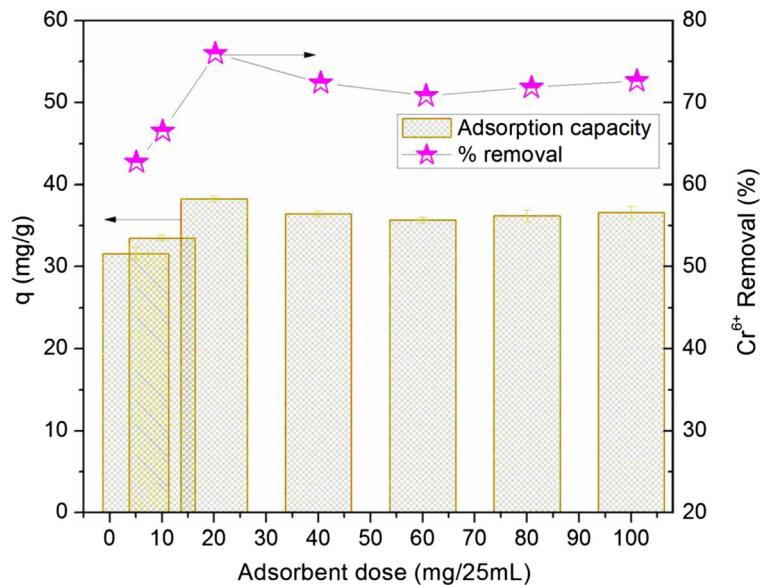
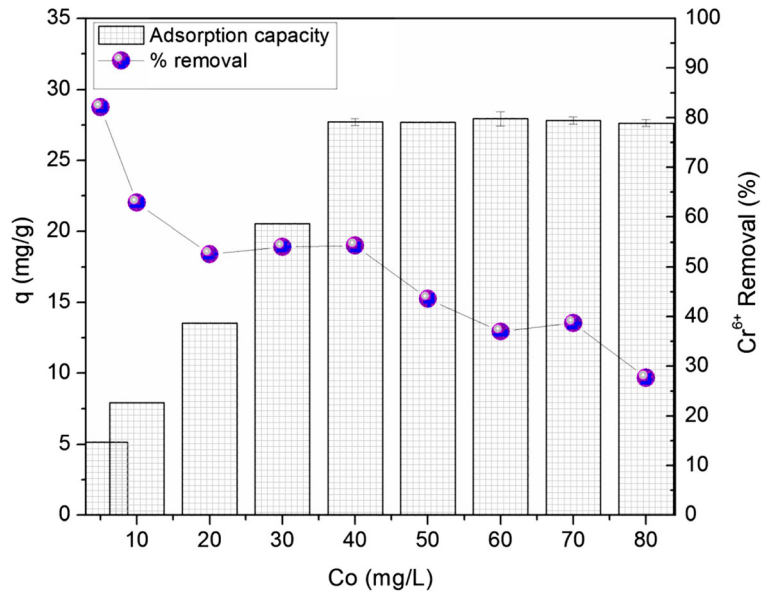


Fig. 9 Effect of initial Cr(VI) concentration on the adsorption capacity and removal efficiency of Cr(VI) by AgNPs-AC at a pH solution of 4, contact time of 150 min, and an adsorbent dose of 20 mg/25 ml



(almond nutshells) activated carbon was a function of initial metal concentration (Manfe et al. 2013).

3.7 Adsorption Isotherm

The adsorption isotherm equilibrium is essential data to explain the mechanism of the adsorption, and the adsorption isotherms were fitted by the Langmuir, Freundlich, and Temkin models. Figure 10 provides a typical adsorption isotherm plot of q_e against C_e . In this study, several commonly adsorption isotherm models were applied to describe the hexavalent chromium adsorption onto AgNPs-AC. They are the Langmuir (Eq.

3), Freundlich (Eq. 4), and Temkin (Eq. 5) models. The corresponding parameters of those models are summarized in Table 1.

$$q_e = \frac{Q_{max}^0 K_L C_e}{1 + K_L C_e} \tag{3}$$

$$q_e = K_F C_e^n \tag{4}$$

$$q_e = \frac{RT}{b} \ln(A_T C_e) \tag{5}$$

Fig. 10 Adsorption isothermal equilibrium prediction of Cr(VI) onto AgNPs-AC at a contact time of 150 min, AgNPs-AC dose of 20 mg/25 mL, and pH solution of 4 and initial Cr(VI) concentration of 40 mg/L

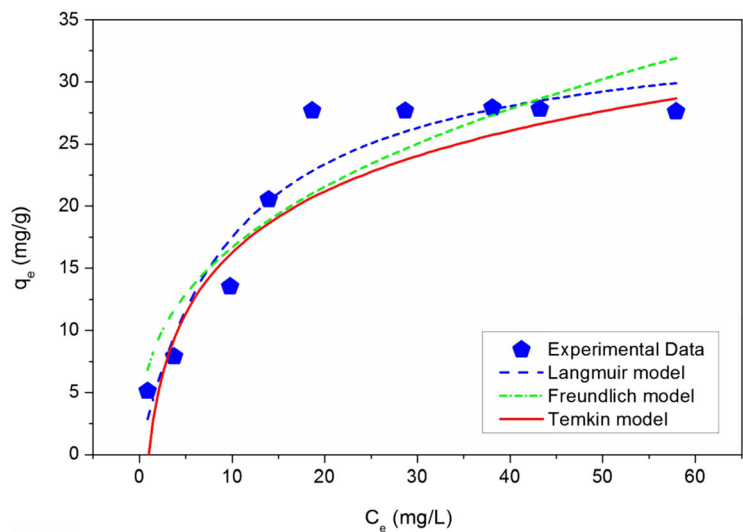


Table 1 Adsorption isothermal parameters and correlation coefficients of the Langmuir, Freundlich and Temkin models for hexavalent chromium adsorption onto AgNPs-AC

The Langmuir model			The Freundlich model			The Temkin model			
q_m	K_L	R^2	K_F	$1/n$	R^2	A_T	b_T	B	R^2
35.09	0.099	0.9121	7.151	0.368	0.835	3.349	98.492	0.460	0.660

where q_e and C_e are obtained from Eq. 1; Q_{\max}^o (mg/g) is the maximum saturated adsorption capacity of adsorbent; K_L (L/mg) is the Langmuir constant related to the affinity between an adsorbent and adsorbate; K_F [(mg/g)/(L/mg)ⁿ] is the Freundlich constant, which characterizes the strength of adsorption; A_T is Temkin isotherm equilibrium binding constant (L/g); b is Temkin isotherm constant; R is universal gas constant (8.314J/mol/K); and T is temperature at 298 K.

The models of Langmuir ($R^2 = 0.9121$) and Freundlich ($R^2 = 0.835$) fit well with the data of hexavalent chromium adsorption onto AgNPs-AC than that of the Temkin model ($R^2 = 0.660$). And the Langmuir was the best model for describing the adsorption isothermal equilibrium of Cr(VI) onto AgNPs-AC. The maximum adsorption capacity (q_m) of AgNPs-AC from the Langmuir model was calculated to be approximately 35.09 mg/g. Besides, the values of the exponent ($1/n$) = 0.368 of the Freundlich model was less than 1 which proved that the adsorption isothermal equilibrium of Cr(VI) onto AgNPs-AC was favorable. And, it can be assumed that adsorption mainly occurs in monolayers or through a fixed number of identical sites on the surface of AgNPs-AC.

3.8 Adsorption Kinetic of AgNPs-AC

In this study, the pseudo-first-order (Eq. 6), pseudo-second-order (PSO Eq. 7), and Elovich (Eq. 8) models were used to describe the adsorption process kinetics of Cr(VI) onto AgNPs-AC. The derivation, meanings, and correct application of such selective models have been discussed in detail by Van et al. (2018a, b).

$$q_t = q_e (1 - e^{-k_1 t}) \quad (6)$$

$$q_t = \frac{q_e^2 k_2 t}{1 + q_e k_2 t} \quad (7)$$

$$q_t = \frac{1}{\beta} \ln(1 + \alpha \beta t) \quad (8)$$

Table 2 presents the calculated kinetic parameters of the pseudo-first-order, pseudo-second-order, and Elovich models from the experimental data. The calculated results showed that the dynamics of hexavalent chromium adsorption fit well to all three above models with R^2 values of 0.8374, 0.9597, and 0.9116, respectively. From Table 2, it can be seen that the pseudo-second-order model provided an excellent correlation coefficient ($R^2 = 0.9597$) with the experimental data in comparison to the pseudo-first-order and Elovich models. The calculated results of the adsorption capacity from both the pseudo-first-order and pseudo-second-order models (14.73 and 16.75 mg/g, respectively) proved that the obtained data from both models were very close to the experimental data ($q_{e, \text{exp}}$ of 15.67 mg/g) in the adsorption of Cr(VI) onto AgNPs-AC. The calculated results suggest that adsorption of Cr(VI) onto AgNPs-AC is controlled by chemisorption, which involves valence forces through sharing or exchange of electrons (Van et al. 2018a, b; Vu et al. 2017). Moreover, the good fit of the data to the model also ascertained that the removal of Cr(VI) by AgNPs-AC is closer to chemisorptions, i.e., new chemical species are generated at the sorbent surface (Wang et al. 2010).

3.9 Adsorption Mechanism Studies

To further elucidate the Cr(VI) adsorption mechanisms on AgNPs-AC, the AC and AgNPs-AC (loaded 2 wt% AgNPs) samples were characterized by SEM, XRD, FTIR, and EDS.

The SEM image in Fig. 1 shows that the structure of the activated carbon-loaded silver nanoparticles (AgNPs-AC 2% w/w) with a negligible increase in surface area of 701.65 m²/g and pore volume of, almost

Table 2 Calculated kinetic parameters of models for Cr(VI) adsorption onto AgNPs-AC

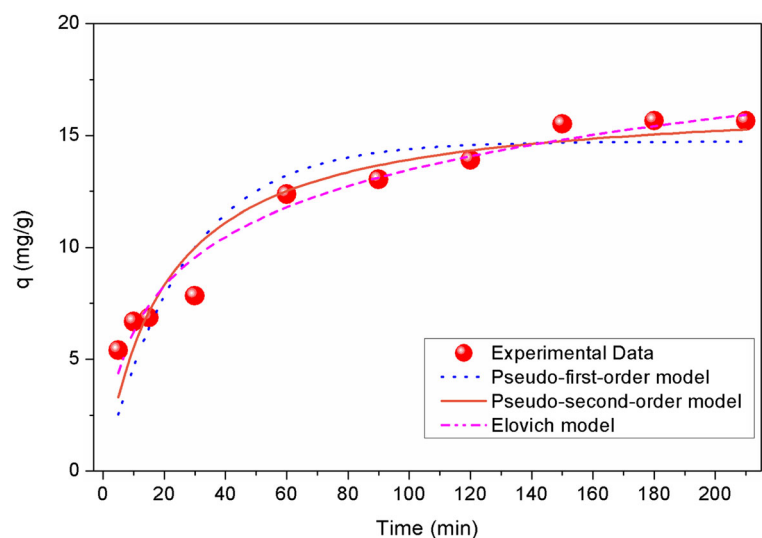
Preudo-first-order			Preudo-second-order			Elovich			$q_{e,exp}$ (mg/g)
$q_{m,cal}$ (mg/g)	K_1	R^2	$q_{m,cal}$ (mg/g)	K_2	R^2	α	β	R^2	
14.73	0.038	0.8374	16.75	2.003	0.9597	1.798	0.297	0.9116	15.67

equal, about $0.061\text{cm}^3/\text{g}$. The surface area and a number of active sites enhance due to the Ag nanoparticles-loaded on the activated carbon (AgNPs-AC) which possesses a crucial role in the adsorption phenomenon (Ghaedi et al. 2018). Therefore, the AgNPs-AC possesses the slightly higher specific surface area than the pristine AC. The results suggested that the AgNPs-loaded play a more important role in Cr(VI) adsorption than the specific surface area of AC. The XRD pattern of the samples are shown in Fig. 2; the observation of typical diffraction peaks of the AC and AgNPs-AC revealed that AgNPs was successfully introduced onto activated carbon that is consistent with the results of SEM and EDS spectra (Fig. 1b, d). Besides, the FTIR analysis indicated the appearance of oxygen-containing functional groups on the AgNPs-AC's surface (i.e., $-\text{OH}$, $-\text{C}=\text{O}$ and $-\text{C}-\text{O}$), especially, the presence of carboxyl groups can contribute to absorb Cr(III) after Cr(VI) was reduced to Cr(III) by positively charged functional groups and an acidic pH (Tran et al. 2017).

Additionally, studies on pH_{PZC} , adsorption isotherm equilibrium and adsorption kinetic by various models were also used to further clearly explain adsorption mechanisms of Cr(VI) onto AgNPs-AC. In the study,

the $\text{pH}_{\text{PZC}} < \text{pH}$ solution further confirmed that there are positively charged functional groups appeared on the AgNPs-AC's surface. And Cr(VI) was easily reduced to Cr(III) by these functional groups. In addition, the acidic medium was superior in Cr(VI) elimination than the basic medium. This may be due to an acidic medium, a positively charged composite leading to easy adsorption of the negative HCrO_4^- ions through electrostatic attraction (Elfeky et al. 2017). The adsorption isotherm equilibrium was fitted best by the Langmuir model, which proved that adsorption mainly occurs in monolayers, or through a fixed number of identical sites on the surface of AgNPs-AC. Meanwhile, the adsorption kinetics fitted best with pseudo-second-order with highest R^2 of 0.9597 with adsorption capacity of 16.75 mg/g that was very close to the experimental data (15.67 mg/g) in adsorption of Cr(VI) onto AgNPs-AC. The calculated results suggest that the adsorption of Cr(VI) onto AgNPs-AC is controlled by chemisorption, which involves valence forces through sharing or exchange of electrons (Van et al. 2018a, b; Vu et al. 2017). Moreover, the good fit of the data to the model also ascertained that the removal of Cr(VI) by AgNPs-AC is closer to chemisorptions, i.e., new chemical species are

Fig. 11 Kinetic models of Cr(VI) adsorption onto AgNPs-AC with an initial Cr(VI) concentration of 40 mg/L, an adsorbent dose of 20 mg/25 mL, pH solution of 4, and contact time of 150 min



generated at the sorbent surface (Wang et al., 2010). However, to further ascertain how much percentage of Cr(VI) was reduced to Cr(III), the later studies need to investigate XPS spectra of AgNPs-AC before and after Cr(VI) adsorption.

4 Conclusion

The commercial activated carbon modified by loading silver nanoparticles (AgNPs-AC) is a fully promising adsorbent for the removal of Cr(VI) from the aqueous solutions. The Cr(VI) adsorption process onto AgNPs-AC was highly depended on pH solution. In this study, the pH of 4 was the optimum condition for the adsorption of Cr(VI) onto AgNPs-AC. The results also showed that there was an increase in the adsorption capacity of Cr(VI) onto AgNPs-AC when the dose of AgNPs-AC and contact time increased. The maximum adsorption capacity of Cr(VI) by AgNPs-AC obtained 27.70 mg/g at 150 min with 20 mg/25 mL of AgNPs-AC dose at 40 mg/L of initial Cr(VI) (Fig. 11). The Langmuir model was the best to describe the adsorption isothermal equilibrium. The adsorption kinetic data were found to fit well with both pseudo-first and pseudo-second-order models with very high correlation coefficients; the mechanism of adsorption was chemisorption due to the appearance of the positively charged groups on AgNPs-AC's surface that reduced Cr(VI) to Cr(III), and Cr(III) was subsequently absorbed by carboxyl groups. Finally, AgNPs-AC was the fully promising adsorbent for the removal of Cr(VI) from the aqueous solution.

Publisher's Note Springer Nature remains neutral with regard to jurisdictional claims in published maps and institutional affiliations.

References

Akram, M., Bhatti, H. N., Iqbal, M., Noreen, S., & Sadaf, S. (2017). Biocomposite efficiency for Cr(VI) adsorption: kinetic, equilibrium and thermodynamics studies. *Journal of Environmental Chemical Engineering*, 5, 400–411.

Ali, A., Saeed, K., & Mabood, F. (2016). Removal of chromium (VI) from aqueous medium using chemically modified banana peels as efficient low-cost adsorbent. *Alexandria Engineering Journal*, 55, 2933–2942.

Altintig, E., Arabaci, G., & Altundag, H. (2016). Preparation and characterization of the antibacterial efficiency of silver loaded

activated carbon from corncobs. *Surface and Coatings Technology*, 304, 63–67.

Alvarez, P., Blanco, C., & Granda, M. (2007). The adsorption of chromium (VI) from industrial wastewater by acid and base-activated lignocellulosic residues. *Journal of Hazardous Materials*, 144, 400–405.

Álvarez-Ayuso, E., García-Sánchez, A., & Querol, X. (2007). Adsorption of Cr(VI) from synthetic solutions and electroplating wastewaters on amorphous aluminium oxide. *Journal of Hazardous Materials*, 142, 191–198.

Anisuzzaman, S. M., Joseph, C. G., Taufiq-Yap, Y. H., Krishnaiah, D., & Tay, V. V. (2015). Modification of commercial activated carbon for the removal of 2,4-dichlorophenol from simulated wastewater. *Journal of King Saud University - Science*, 27, 318–330.

Berihun, D. (2017). Removal of chromium from industrial wastewater by adsorption using coffee husk. *Journal of Material Sciences & Engineering*, 6, 1–6.

De Castro, M. L. F. A., Abad, M. L. B., Sumalinog, D. A. G., Abarca, R. R. M., Paoprasert, P., & de Luna, M. D. G. (2018). Adsorption of methylene blue dye and Cu(II) ions on EDTA-modified bentonite: isotherm, kinetic and thermodynamic studies. *Sustainable Environment Research*, 28, 197–205.

Demir, A., & Arisoy, M. (2007). Biological and chemical removal of Cr(VI) from waste water: cost and benefit analysis. *Journal of Hazardous Materials*, 147, 275–280.

Elfeky, S. A., Mahmoud, S. E., & Youssef, A. F. (2017). Applications of CTAB modified magnetic nanoparticles for removal of chromium (VI) from contaminated water. *Journal of Advanced Research*, 8, 435–443.

EPA. (1983). Methods for chemical analysis of water and wastes. In *United States Environmental Protection Agency*.

Foo, K. Y., & Hameed, B. H. (2009). Utilization of biodiesel waste as a renewable resource for activated carbon: application to environmental problems. *Renewable and Sustainable Energy Reviews*, 13, 2495–2504.

Ghaedi, M., Ramazani, & Roosta, M. (2011). Gold nanoparticle loaded activated carbon as novel adsorbent for the removal of Congo red. *Indian Journal of Science and Technology*, 4, 1208–1217.

Ghaedi, M., Roosta, M., Ghaedi, A. M., Ostovan, A., Tyagi, I., Agarwal, S., & Gupta, V. K. (2018). Removal of methylene blue by silver nanoparticles loaded on activated carbon by an ultrasound-assisted device: optimization by experimental design methodology. *Research on Chemical Intermediates*, 44, 2929–2950.

Huang, Z.-N., Wang, X.-l., & Yang, D.-S. (2015). Adsorption of Cr(VI) in wastewater using magnetic multi-wall carbon nanotubes. *Water Science and Engineering*, 8, 226–232.

Jain, M., Yadav, M., Kohout, T., Lahtinen, M., Garg, V. K., & Sillanpää, M. (2018). Development of iron oxide/activated carbon nanoparticle composite for the removal of Cr(VI), Cu(II) and Cd(II) ions from aqueous solution. *Water Resources and Industry*, 20, 54–74.

Kakavandi, B., Kalantary, R. R., Farzadkia, M., Mahvi, A. H., Esrafil, A., Azari, A., Yari, A. R., & Javid, A. B. (2014). Enhanced chromium (VI) removal using activated carbon modified by zero valent iron and silver bimetallic nanoparticles. *Journal of Environmental Health Science & Engineering*, 12, 115–115.

- Karimi, H. (2012). Silver nanoparticle loaded on activated carbon as efficient adsorbent for removal of methyl orange. *Indian Journal of Science and Technology*, 5, 2346–2353.
- Kera, N. H., Bhaumik, M., Pillay, K., Ray, S. S., & Maity, A. (2017). Selective removal of toxic Cr(VI) from aqueous solution by adsorption combined with reduction at a magnetic nanocomposite surface. *Journal of Colloid and Interface Science*, 503, 214–228.
- Kumar, A., & Jena, H. M. (2017). Adsorption of Cr(VI) from aqueous phase by high surface area activated carbon prepared by chemical activation with ZnCl₂. *Process Safety and Environmental Protection*, 109, 63–71.
- Kumar, S., & Meikap, B. C. (2014). Removal of chromium(VI) from waste water by using adsorbent prepared from green coconut shell. *Desalination and Water Treatment*, 52, 3122–3132.
- Lazim, Z. M., Hadibarata, T., Puteh, M. H., & Yusop, Z. (2015). Adsorption characteristics of bisphenol a onto low-cost modified phyto-waste material in aqueous solution. *Water, Air, & Soil Pollution*, 226.
- Li, H., Dong, X., da Silva, E. B., de Oliveira, L. M., Chen, Y., & Ma, L. Q. (2017). Mechanisms of metal sorption by biochars: biochar characteristics and modifications. *Chemosphere*, 178, 466–478.
- Lu, H., Wang, J., Hao, H., & Wang, T. (2017). Magnetically separable MoS₂/Fe₃O₄/nZVI nanocomposites for the treatment of wastewater containing Cr(VI) and 4-Chlorophenol. *Nanomaterials (Basel)*, 7.
- Manfè, M., Attar, S., Parande, M., & Topare, N. (2013). Treatment of Cr(VI) contaminated waste water using biosorbent *Prunus amygdalus* (almond) nut shell carbon. *International Journal of Chemical Science*, 10(2), 609–618.
- Manzoor, Q., Nadeem, R., Iqbal, M., Saeed, R., & Ansari, T. M. (2013). Organic acids pretreatment effect on Rosa bourbonia phyto-biomass for removal of Pb(II) and Cu(II) from aqueous media. *Bioresource Technology*, 132, 446–452.
- Marahel, F., Ghaedi, M., & Ansari, A. (2015). Zinc oxide nanoparticles loaded on activated carbon and its application for adsorption removal of uric acid. *Synthesis and Reactivity in Inorganic, Metal-Organic, and Nano-Metal Chemistry*, 45, 1387–1395.
- Mitra, S., Sarkar, A., & Sen, S. (2017). Removal of chromium from industrial effluents using nanotechnology: a review. *Nanotechnology for Environmental Engineering*, 2(11), 1–14.
- Owalude, S. O., & Tella, A. C. (2016). Removal of hexavalent chromium from aqueous solutions by adsorption on modified groundnut hull. *Beni-Suef University Journal of Basic and Applied Sciences*, 5, 377–388.
- Rai, M. K., Shahi, G., Meena, V., Meena, R., Chakraborty, S., Singh, R. S., & Rai, B. N. (2016). Removal of hexavalent chromium Cr(VI) using activated carbon prepared from mango kernel activated with H₃PO₄. *Resource-Efficient Technologies*, 2, S63–S70.
- Saha, R., Nandi, R., & Saha, B. (2011). Sources and toxicity of hexavalent chromium. *Journal of Coordination Chemistry*, 64, 1782–1806.
- Salem, I. A., Fayed, T. A., El-Nahass, M. N., & Dawood, M. (2018). A comparative study for adsorption of methylene blue dye from wastewater on to three different types of rice ash. *Journal of Pharmaceutical and Applied Chemistry*, 4, 99–107.
- Sheth, D., & M Soni, V. (2005). Comparative study of removal of Cr(VI) with PAC. *GAC and adsorbent prepared from tobacco stems*, 47, 218–221.
- Singh, S. K. (2017). Removal of hexavalent chromium Cr(VI) by using sugarcane bagasse. *Indian Journal of Scientific Research*, 13, 73–76.
- Tang, C., Hu, D., Cao, Q., Yan, W., & Xing, B. (2017). Silver nanoparticles-loaded activated carbon fibers using chitosan as binding agent: preparation, mechanism, and their antibacterial activity. *Applied Surface Science*, 394, 457–465.
- Tran, H. N., You, S.-J., & Chao, H.-P. (2016). Effect of pyrolysis temperatures and times on the adsorption of cadmium onto orange peel derived biochar. *Waste Management & Research*, 34(2), 129–138.
- Van, H. T., Bui, T. T. P., & Nguyen, L. H. (2018a). Residual organic compound removal from aqueous solution using commercial coconut Shell activated carbon modified by a mixture of seven metal salts. *Water, Air, & Soil Pollution*, 229.
- Van, H. T., Nguyen, T. M. P., Thao, V. T., Vu, X. H., & Nguyen, L. H. (2018b). Applying activated carbon derived from coconut shell loaded by silver nanoparticles to remove methylene blue in aqueous solution. *Water Air Soil Pollution*, 229, 393.
- Vu, T. M., Trinh, V. T., Doan, D. P., Van, H. T., Nguyen, T. V., Vigneswaran, S., & Ngo, H. H. (2017). Removing ammonium from water using modified corncob-biochar. *The Science of the Total Environment*, 579, 612–619.
- Wang, X. S., Chen, L. F., Li, F. Y., Chen, K. L., Wan, W. Y., & Tang, Y. J. (2010). Removal of Cr (VI) with wheat-residue derived black carbon: reaction mechanism and adsorption performance. *Journal of Hazardous Materials*, 175, 816–822.